

MIT Open Access Articles

Ultrafast 2D IR anisotropy of water reveals reorientation during hydrogen-bond switching

The MIT Faculty has made this article openly available. **Please share** how this access benefits you. Your story matters.

Citation: Ramasesha, Krupa et al. "Ultrafast 2D IR Anisotropy of Water Reveals Reorientation During Hydrogen-bond Switching." *The Journal of Chemical Physics* 135.5 (2011): 054509. © 2011 American Institute of Physics

As Published: <http://dx.doi.org/10.1063/1.3623008>

Publisher: American Institute of Physics (AIP)

Persistent URL: <http://hdl.handle.net/1721.1/73989>

Version: Author's final manuscript: final author's manuscript post peer review, without publisher's formatting or copy editing

Terms of use: Creative Commons Attribution-Noncommercial-Share Alike 3.0



Ultrafast 2D IR Anisotropy of Water Reveals Reorientation during Hydrogen-Bond Switching

Krupa Ramasesha, Sean T. Roberts¹, Rebecca A. Nicodemus, Aritra Mandal and Andrei Tokmakoff*

*Department of Chemistry and George R. Harrison Spectroscopy Laboratory,
Massachusetts Institute of Technology, Cambridge, MA 02139 USA*

Abstract: Rearrangements of the hydrogen bond network of liquid water are believed to involve rapid and concerted hydrogen bond switching events, during which a hydrogen bond donor molecule undergoes large angle molecular reorientation as it exchanges hydrogen-bonding partners. To test this picture of hydrogen bond dynamics, we have performed ultrafast 2D IR spectral anisotropy measurements on the OH stretching vibration of HOD in D₂O to directly track the reorientation of water molecules as they change hydrogen bonding environments. Interpretation of the experimental data is assisted by modeling drawn from molecular dynamics simulations, and we quantify the degree of molecular rotation on changing local hydrogen bonding environment using restricted rotation models. From the inertial 2D anisotropy decay, we find that water molecules initiating from a strained configuration and relaxing to a stable configuration are characterized by a distribution of angles, with an average reorientation half-angle of 10°, implying an average reorientation for a full switch of $\geq 20^\circ$. These results provide evidence that water hydrogen bond network connectivity switches through concerted motions involving large angle molecular reorientation.

tokmakot@mit.edu

¹ Present address: Department of Chemistry, University of Southern California, Los Angeles, CA 90089

I. Introduction

The rapidly evolving structure of liquid water's hydrogen bond (HB) network is at the heart of aqueous physical processes, such as ion solvation, the hydrophobic effect, proton transport, chemical reactivity, and biological processes. While there is consensus over most time and spatially averaged characteristics of water, the underlying HB dynamics responsible for water's anomalous properties remain difficult to describe. Water's directional HB network undergoes femtosecond local fluctuations and picosecond structural reorganization.¹ It is believed that HB rearrangement is a cooperative event involving the reorganization of multiple hydrogen bonded molecules,² a concept originally framed as transitions between "inherent structures".^{3,4} Although difficult to verify, experiments recently provided evidence that a HB donor molecule switches between HB acceptors in a single concerted process, passing through a bifurcated transition state.⁵⁻⁷ Further, simulations of water models⁸⁻¹⁰ and experiments on switching of HBs to solvated ions^{11,12} indicate that hydrogen bond connectivity changes by large angle jump reorientation. Classical molecular dynamics (MD) simulations describe the fluctuations in HB donor and acceptor coordination number that enable the formation of a bifurcated HB transition state, and exhibit an average jump angle of 68°.⁸ Other less probable switching mechanisms in simulations have also been described,¹³ but all proposed mechanisms of HB exchange involve a large angle reorientation of the switching water molecule.

Here we present experimental evidence for the picture of ultrafast HB switching by large angle reorientation in water. To describe the degree of reorientation of a water molecule while shifting HB environments, we use ultrafast two-dimensional infrared (2D

IR) spectroscopy of the OH stretching vibration of dilute HOD in D₂O.^{14,15} The OH stretch vibrational frequency ($\langle\omega_{\text{OH}}\rangle = 3400 \text{ cm}^{-1}$) is a sensitive reporter of HB environment, with lower (red) frequencies ($\omega_{\text{OH}} < 3400 \text{ cm}^{-1}$) corresponding to water molecules in strong, linear hydrogen bonded configurations, and higher (blue) frequencies ($\omega_{\text{OH}} > 3500 \text{ cm}^{-1}$) corresponding to those in broken or strained hydrogen bonded configurations (non-HB or NHB).¹⁴⁻¹⁶ 2D IR spectroscopy provides the ability to correlate time-evolving spectral features and chemical exchange with ultrafast time resolution. Previous 2D IR experiments have shown that water molecules in NHB configurations undergo inertial relaxation to stable HB configurations within 150 fs, indicating a concerted hydrogen bond switching process and the absence of dangling HBs in water.⁵ While ω_{OH} shows reasonable correlation with hydrogen bond length, its correlation with hydrogen bond angle is weak, especially for the large angles that exist during HB switching.¹⁵ Therefore, we employ polarization-sensitive 2D IR measurements to characterize changes in OH transition dipole orientation during HB fluctuations and rearrangements.¹⁷

The recent proposal that HB rearrangement involves large angle molecular reorientation, leads to the prediction that time-dependent ω_{OH} spectral shifts during hydrogen bond exchange should be correlated with inertial OH rotation.^{7,9} Information on ultrafast molecular reorientation is commonly obtained in the form of a rotational anisotropy, $r(\tau) = 0.4 P_2\langle\boldsymbol{\mu}(\tau)\cdot\boldsymbol{\mu}(0)\rangle$, that is extracted from polarization sensitive experiments, where P_2 is the second Legendre polynomial orientational correlation function and $\boldsymbol{\mu}(\tau)$ is the orientation of the molecular dipole at a given time τ . Simulations and pump-probe (PP) measurements have revealed a dependence of the inertial

anisotropy decay on detection frequency.^{14,18-21} However, pump-probe anisotropy measurements cannot correlate anisotropy with both initial and final hydrogen bond configuration with high enough time resolution to follow hydrogen bond switching. To overcome these obstacles, we made measurements of the 2D IR spectral anisotropy as a function of both excitation and detection frequency to study the inertial orientational dynamics of water. Earlier measurements of the 2D anisotropy of aqueous ions^{11,12} and calculations of the 2D anisotropy of water^{7,9} have revealed the advantage of the technique in understanding the rotational dynamics of water. 2D IR anisotropy is related to the joint probability of exciting the OH oscillator at a frequency ω_1 and observing an anisotropy r at frequency ω_3 , after a waiting time τ_2 . The results presented here provide clear signatures of heterogeneous reorientational motion on timescales <400 fs. Simulation of the experiment with a well characterized water model allows us to interpret the origin of the spectrally varying anisotropy in terms of specific dynamic events. Further, we quantify the average angular changes experienced by different configurations during the inertial period, providing evidence that the rapid return of NHB configurations to hydrogen bonded geometries is associated with large angle reorientation.

II. Methods

IIa. Experimental

Experiments used a home-built optical parametric amplifier which generates 45 fs pulses centered at 3400 cm^{-1} , having a 350 cm^{-1} bandwidth with pulse energy of $5\text{ }\mu\text{J}$, as detailed in Ref. 22. For the double-differential 2D IR anisotropy measurements, we constructed a pump-probe Fourier transform 2D interferometer²³ that provided

simultaneous balanced detection of parallel (ZZZZ) and perpendicular (YYZZ) spectra. A ~5% reflection of the IR beam was split to make the probe pulse, which was sent to a delay stage for scanning the waiting time (τ_2). The remaining IR beam was equally split and recombined in a Mach-Zehnder interferometer to create the collinear pump pair for the 2D experiment. One of the pump beams was sent to a delay stage (Aerotech), and stepped in 2 fs intervals until 400 fs, to generate the excitation (τ_1) axis. The other fixed pump beam was chopped at half the laser repetition rate. The beams were focused and crossed in the sample, with a spot size of 100 μm at the sample.

The HOD/D₂O sample was made by adding ~1% by volume of H₂O (de-ionized, 18 M Ω resistance) to D₂O (99.96% purity from Cambridge Isotope Laboratories, Inc.), such that the OH stretch absorbance at 3400 cm^{-1} was always kept below 0.4 to minimize re-absorption contributions to the signal. For acquiring 2D IR anisotropy, the HOD/D₂O sample was held between 1 mm thick CaF₂ windows, with a path length of 100 μm . Due to non-resonant effects from CaF₂ windows, we show 2D IR anisotropy for $\tau_2 > 100$ fs. To acquire dispersed pump-probe spectra, we simply blocked the non-chopped pump beam and scanned the probe beam. For the dispersed pump-probe experiments, the sample was held between 100 nm thick Si₃N₄ windows (Norcada) to eliminate non-resonant signal, allowing us to access <100 fs time delays.

Tunable zero-order half-waveplates (Alphas) and wire-grid polarizers (Molelectron) controlled the polarization of each beam, and were calibrated with respect to an analyzing polarizer placed at the sample position prior to data collection. The polarizations of the two pump beams were oriented at 0° (*Z*) and the probe was oriented at 45° with respect to the pump beams. After passing through the sample, the probe is

split into two arms with a 50/50 beamsplitter. One arm passed through a polarizer oriented parallel (*Z*) to the pump beams to acquire *ZZZZ* surfaces, and the other arm passed through a polarizer oriented perpendicular to the pump beams (*Y*) to acquire *YYZZ* surfaces. Each of the two arms was dispersed in a monochromator and imaged onto one stripe of a 2 x 64 element liquid nitrogen cooled MCT array (Infrared Systems) with a 16 cm⁻¹/pixel resolution, which provided the ω_3 dimension of the 2D IR spectrum. After the analyzing polarizer in the perpendicular arm of the probe, a waveplate-polarizer pair was used to rotate the probe to 0° to ensure that the detected spectra were free of artifacts due to the polarization dependence of the grating diffraction efficiency. We also normalize for pixel sensitivities between the two stripes of the array before calculating anisotropy by multiplying the signal on one of the stripes by the ratio of the probe spectra from the two stripes.

The *ZZZZ* and *YYZZ* τ_1 - ω_3 surfaces were Fourier transformed in the τ_1 dimension to obtain the absorptive (real) 2D IR spectra. Prior to this transformation, the constant pump-probe background in the τ_1 dimension arising from the chopped pump beam and the probe beam was subtracted, and a Hanning window was applied in τ_1 to minimize noise. The error in determining τ_1 (± 5 fs) was corrected for by adding a phase factor²⁴ during Fourier transformation upon invoking the projection-slice theorem.^{25,26} At any given waiting time, this τ_1 correction factor was found to be the same for both the *ZZZZ* and *YYZZ* surfaces since they were acquired simultaneously. At every waiting time, the pump-probe or 2D anisotropy was obtained from the corresponding parallel (S_{ZZZZ}) and perpendicular (S_{YYZZ}) detected spectra using, $r = (S_{ZZZZ} - S_{YYZZ}) / (S_{ZZZZ} + 2S_{YYZZ})$. A Kramers-Kronig assumption was used to obtain the

imaginary part of the 2D spectrum and the 2D power spectrum.^{27,28} 2D anisotropy surfaces were then calculated for each (ω_1, ω_3) point for both real and power spectra. In this paper, we present one set of data obtained from averaging 4-6 surfaces at every waiting time, for each polarization geometry. This data set is representative of all the 2D anisotropy spectra we have taken on this system.

We corrected for the thermally shifted ground state (TSGS) in the dispersed pump-probe data using a method very similar to those outlined in Refs. 29-31. Using the *ZZZZ* and *YYZZ* dispersed pump-probe spectra at our longest waiting time of 8.5 ps, we calculated the isotropic TSGS spectrum. We let the TSGS spectrum grow mono-exponentially with a 2 ps timescale. We found that including an intermediate state²⁹ for the OH stretch relaxation had negligible effect on the <100 fs inertial dynamics. We subtracted the TSGS spectrum at every waiting time from both *ZZZZ* and *YYZZ* spectra and proceeded to calculate dispersed pump-probe anisotropy from these corrected spectra. The librational dynamics we see on <100 fs timescale were insensitive to the picosecond timescale that characterized the growth of the TSGS. TSGS contributions to 2D IR anisotropy were found to be negligible at <1 ps waiting times, and therefore the 2D anisotropy data reported in this paper do not include this correction.

IIb. Simulations and Modeling

To assist in the interpretation of experimental data, we modeled the 2D IR and pump-probe anisotropy of HOD/D₂O using molecular dynamics simulations of SPC/E water and a mixed quantum-classical model for the OH vibrational spectroscopy that has been described elsewhere.¹⁵ From the simulations, we extract instantaneous frequencies

$\omega_{\text{OH}}(t)$ and the projection of the OH bond orientation onto the $i = x, y$ and z coordinates. Similar to prior calculations,^{14,15,32} we assume that the OH transition dipole is oriented along the OH bond axis and we account for the non-Condon effects by scaling the magnitude of the OH transition dipole based on an empirical mapping between it and the frequency of the OH bond: $\mu_{i,ab} = \hat{i} \cdot \hat{\mu} \langle a | \mu(\omega_{ab}) | b \rangle$.³³ The trajectories are used to calculate rephasing (–) and non-rephasing (+) third order response functions^{34,35} according to the semiclassical approximation.³³

$$\begin{aligned}
R_{\pm,ijj}^{(3)}(\tau_1, \tau_2, \tau_3) = & \text{Re} \left[2 \left\langle \mu_{10,i}(\tau_1 + \tau_2 + \tau_3) \mu_{10,i}(\tau_1 + \tau_2) \mu_{10,j}(\tau_1) \mu_{10,j}(0) \right. \right. \\
& \times \exp \left[\pm i \int_0^{\tau_1} \omega_{10}(\tau) d\tau + i \int_{\tau_1 + \tau_2}^{\tau_1 + \tau_2 + \tau_3} \omega_{10}(\tau') d\tau' \right] \left. \right\rangle \\
& - \left\langle \mu_{21,i}(\tau_1 + \tau_2 + \tau_3) \mu_{21,i}(\tau_1 + \tau_2) \mu_{10,j}(\tau_1) \mu_{10,j}(0) \right. \\
& \left. \times \exp \left[\pm i \int_0^{\tau_1} \omega_{10}(\tau) d\tau + i \int_{\tau_1 + \tau_2}^{\tau_1 + \tau_2 + \tau_3} \omega_{21}(\tau') d\tau' \right] \right\rangle \left. \right] \quad (1)
\end{aligned}$$

These two terms describe the time-dependent coupled vibrational-orientational dynamics for the $v = 0-1$ and $v = 1-2$ energy gaps that are resonant with the sequence of pulses in our experiments. Parallel ($S_{//}$) and perpendicular (S_{\perp}) 2D IR spectra are obtained by averaging all the parallel and perpendicular components of the signal, $S_{//} = (S_{xxxx} + S_{yyyy} + S_{zzzz})/3$ and $S_{\perp} = (S_{yyzz} + S_{xxzz} + S_{yyxx})/3$. Both rephasing and non-rephasing signals for each geometry are summed, Fourier transformed with respect to τ_1 and τ_3 to obtain 2D IR spectra, and used to calculate 2D anisotropy surfaces.

III. Results and Discussion

IIIa. Pump-Probe Anisotropy of HOD/D₂O

As an initial characterization of the inertial OH reorientation, we performed dispersed pump-probe anisotropy experiments with broadband excitation. These measurements follow the reorientation of water molecules that initiate at all possible HB configurations and are detected at frequencies (ω_3) corresponding to certain HB environments, after a waiting time, τ_2 . Figure 1a displays the ZZZZ and YZZZ dispersed pump-probe spectra before TSGS correction, and Figure 1b shows slices of the dispersed pump-probe at 3400 cm⁻¹, following TSGS correction. Figure 2 shows time traces of pump-probe anisotropy at three detection frequencies, from experiment and simulation. Much like the broadband pump-probe anisotropy with integrated detection, transients at all detection frequencies showed bimodal relaxation corresponding to the inertial reorientation of the HOD molecule followed by collective molecular reorientation.³⁶ We find that the timescales observed are independent of detection frequency, but the relative amplitude of the components varies. After correcting for the thermally shifted ground state as described earlier, the experimental data were fit to double exponential decays with fixed timescales of 70 fs and 2.7 ps. These timescales agree with earlier measurements of the integrated pump-probe anisotropy.^{30,36} We find that the amplitude of the inertial decay (A) increases monotonically with detection frequency ω_3 (Figure 2, lower left panel), indicating that molecules detected in strained configurations have experienced more orientational randomization during the inertial time-period than those detected in strong hydrogen bond configurations.^{14,30}

Inertial reorientation includes rotational motion due to fluctuations about hydrogen bonded configurations and reorientation during hydrogen bond switching. Since these motions occur within a hindered environment, the orientational relaxation is incomplete until the global structure of the liquid reorganizes. We can quantify the degree of orientational motion of the OH transition dipole during the inertial period within the framework of restricted rotation models.³⁷⁻³⁹

We study two models of restricted reorientation, which are described in terms of the restricted orientational probability distribution $p(\theta)$, that defines the angular configurations allowed during inertial relaxation. The upper panel of Figure 3 shows the potentials of mean force for the hard cone and the harmonic cone probability distributions. From these models, we obtain the generalized order parameter, S , which characterizes the extent of angular motion during the inertial period

$$S = \left[\int d\Omega p(\theta) P_2(\cos \theta) \right] / \left[\int d\Omega p(\theta) \right] \quad (2)$$

Here, Ω refers to spherical coordinates (θ, ϕ) and $\int d\Omega = \int d\phi \int \sin \theta d\theta$. In the harmonic cone model,¹⁸ the degree of restricted rotation is characterized by θ_H as described by $p(\theta) = \exp[-\theta^2/2\theta_H^2]$. For the hard cone model³⁷⁻³⁹, $p(\theta)$ imposes an abrupt angular cut-off to orientational excursions greater than the half-cone angle θ_0 . The generalized order parameter for the hard cone model can be simplified to,

$$S_{HC} = \frac{\int_0^{2\pi} d\phi \int_0^{\theta_0} \sin \theta \cdot P_2(\cos \theta) \cdot d\theta}{\int_0^{2\pi} d\phi \int_0^{\theta_0} \sin \theta \cdot d\theta} = \frac{\cos \theta_0 (1 + \cos \theta_0)}{2} \quad (3)$$

Since the amplitude of the fast anisotropy decay, A , is the residual anisotropy following inertial relaxation, we equate $A=1-S^2$, and use S to determine θ_0 and θ_H for both restricted reorientation models. The average angular deviations during the inertial period can be obtained using the mean half-cone angle

$$\langle \theta \rangle = \left[\int d\Omega \theta p(\theta) \right] / \left[\int d\Omega p(\theta) \right], \quad (4)$$

whereas the extent of large excursions in angle can be quantified through the half-cone angle θ_0 , or through $2\theta_H$, the half-angle that contains 95% of inertial angular excursions. We found that the calculated $\langle \theta \rangle$ for both the harmonic cone and hard cone model were nearly identical, and that the deduced hard cone angle was the same as the two standard deviations in the harmonic cone model, $2\theta_H \approx \theta_0$. For this reason we only report angular changes in terms of the harmonic cone model.

Figure 3 displays the average OH angular changes and large excursions during the inertial period as a function of detection frequency ω_3 . The experimental mean angular changes for the harmonic and hard cone models show a modest increase with ω_3 , from $\sim 7^\circ$ at 3380 cm^{-1} to $\sim 12^\circ$ at 3550 cm^{-1} , and the $2\theta_H$ excursions vary from $\sim 10^\circ$ to $\sim 23^\circ$ over the same range. The $2\theta_H$ values are lower than the angles that Bakker and co-workers calculated by applying a hard cone model to their narrowband pump-probe anisotropy of HOD/D₂O, where they report a 20-28° range.²⁰ However, the average harmonic cone angles are similar to those that Moilanen et al. calculated for the OD stretch of HOD/H₂O from broadband pump-probe measurements.¹⁸ These observations demonstrate that, upon inertial relaxation, molecules detected in stable HB configurations undergo reorientation to a lesser extent than those detected in strained configurations.

For free rotation, the harmonic cone angle can be related to the HOD moment of inertia I and the angular frequency ω_{rot} by $\theta_H^2 = k_B T / I \omega_{rot}^2$.¹⁸ Using the value $I = 2.847 \times 10^{-47} \text{ kg m}^2$, angular frequencies are calculated to vary from $\sim 670\text{-}330 \text{ cm}^{-1}$, as a function of increasing detection frequency ω_3 . The frequency range agrees with the broad infrared signature of the HOD librational band.⁴⁰⁻⁴⁴

IIIb. 2D IR Anisotropy of HOD/D₂O

A waiting time series of $ZZZZ$ and $YYZZ$ 2D IR spectra are displayed in Figure 4. Both polarizations show an asymmetrically broadened lineshape at early waiting times as described previously.^{5,24} The increased antidiagonal line width for blue side excitation reflects the <150 fs spectral relaxation of NHB species toward stable hydrogen bond configurations, and the lack of any persistent dangling HB species. The differences in lineshapes between $S_{//}$ and S_{\perp} are subtle, with the most visible difference being the smaller slope of the node between the positive $v = 0\text{-}1$ and negative $v = 1\text{-}2$ transitions in perpendicular spectra. Since the nodal slope is a measure of loss of frequency correlation,⁴⁵⁻⁴⁷ the difference between $ZZZZ$ and $YYZZ$ surfaces points to a correlation of frequency and orientational HB dynamics.

2D anisotropies can be calculated from a number of representations, of which those obtained from 2D IR absorptive and 2D IR power spectra for $\tau_2=250$ fs are compared in Figure 5. As a result of the positive and negative features in the absorptive spectrum, the resulting 2D anisotropy contains distortions that arise from the singularity along the nodal line. For this reason we also analyze the anisotropy obtained from 2D power spectra, which retains a similar anisotropy profile without the distortions near the

node. Comparison of the anisotropy profiles, with contour lines placed at anisotropy intervals of 0.01, provide an estimate of the degree of uncertainty that exists in quantitatively interpreting the data. Representative 2D IR anisotropies obtained from measured real spectra are shown in Figure 6a for four waiting times. The anisotropy is color coded and the underlying lineshape of the isotropic spectrum, $S_{iso} = (S_{||} + 2S_{\perp})/3$, is represented by solid contour lines. The corresponding anisotropies obtained from power spectra are shown in Figure 7a. We analyze relaxation within four quadrants of the 2D anisotropy, which vary by excitation and detection frequency, referring to frequencies $<3400 \text{ cm}^{-1}$ as “red” and frequencies $>3500 \text{ cm}^{-1}$ as “blue”.

Formally the 2D anisotropy is related to a four-point joint correlation function in the OH dipole moment.^{48,49} It remains a challenge to interpret nonlinear spectra in which rotational and vibrational degrees of freedom are coupled, since general models for this case have not yet been established. To initially simplify the analysis, we make the approximation that reorientational and vibrational dynamics during τ_1 and τ_3 are negligible, so that rotation can be completely described in terms of the two-point correlation function $\langle P_2[\mu(\tau_2) \cdot \mu(0)] \rangle$. We use restricted rotation modeling to provide quantitative estimates of the angular deviations of water molecules upon changing HB environment. To this end, we equate the residual anisotropy values from the four quadrants of the 2D anisotropy surface following the inertial decay ($\tau_2 = 100 \text{ fs}$) to the square of the generalized order parameter, S^2 .

Along the diagonal, the 2D anisotropy obtained from both real and power spectra drops from red to blue, indicating that water molecules in strong HB configurations are more orientationally constrained than those in strained and bifurcated configurations. The

red-to-red ($\omega_1 = \text{red}, \omega_3 = \text{red}$) region corresponds to molecules that persist in stable HB configurations, and the value of $r = 0.4$ at $\tau_2 = 100$ fs indicates that these molecules do not reorient during the inertial period (within our experimental uncertainty in r of $\pm 5\%$). The blue-to-blue region, which corresponds to molecules that initiate and end in unstable configurations, shows the most orientational randomization.

Off-diagonal regions of the 2D anisotropy reflect orientational changes that accompany shifts in HB environment. In the blue-to-red region of the 2D anisotropy, we probe molecules that initiate in unstable configurations, including those undergoing HB switching, large amplitude librations, and hydrogen bond extension, and subsequently relax to a stable HB configuration. In this region of the 2D anisotropy from both real and power spectra, inertial relaxation is characterized by the anisotropy value of 0.37 for $(\omega_1, \omega_3) = (3550 \text{ cm}^{-1}, 3350 \text{ cm}^{-1})$ at $\tau_2 = 100$ fs, which corresponds to average rotational relaxation of $\langle \theta \rangle \sim 10^\circ$. Since this corresponds to relaxation of an unstable NHB configuration to a HB configuration, the angle represents half the full extent of orientational excursion. Given that this angle averages over successful and non-successful switches and translational HB fluctuations, this implies that water molecules shifting from strained to stable hydrogen bonding environment reorient by a mean angle of at least 20° , with HB switching angles probably being considerably larger. The $\tau_2 = 100$ fs red-to-blue anisotropy calculated from power spectra, obtained for $(\omega_1, \omega_3) = (3350 \text{ cm}^{-1}, 3550 \text{ cm}^{-1})$ leads to $\langle \theta \rangle \sim 5^\circ$, which is smaller than the angles we obtained in the blue-red quadrant. The red-to-blue anisotropy calculated from real spectra show

larger angles of $\sim 10^\circ$, but due to low signal-to-noise in this quadrant of the real spectra, we place large error bars on these numbers.

On longer timescales, the 1 ps blue-to-red anisotropy of 0.28 from power spectra indicates that OH dipoles initially in NHB configurations diffuse to sample an average half-cone angle of $\sim 18^\circ$ within the first picosecond. Blue-to-red anisotropy of 0.3 from real spectra, similarly translates to a $\langle \theta \rangle \sim 17^\circ$. However, those molecules initially excited in strong HB configurations barely change their orientation ($r \sim 0.4$), indicating that there are a significant number of HBs that remain intact for a few picoseconds. Since the 1 ps waiting time is on the order of spectral diffusion timescales for the OH stretch of HOD/D₂O, the contour lines in the 2D anisotropy become almost parallel to the ω_3 axis and equally spaced in ω_1 , indicating that the rate of anisotropy decay is spectrally independent from this time forward. The vertical orientation of these contour lines means that at any given ω_1 , the anisotropy is the same across all ω_3 , suggesting that all water molecules behave similarly after about 1 ps.

Figure 8a shows the waiting time-dependent decay of the anisotropy in each quadrant. As expected, the red-to-red anisotropy remains high at even longer waiting times due to the persistence of stable HBs, while the blue-to-blue anisotropy is relatively low at all waiting times due to the transient NHB species. Anisotropies for molecules initiating blue are consistently lower than for those that initiate red. Figure 9 shows the comparison between the average and largest angles ($2\theta_H$) from the 100 fs 2D anisotropy surfaces using restricted rotation modeling. The angles extracted from the $\omega_1 = 3550 \text{ cm}^{-1}$ slice are larger than those from the $\omega_1 = 3350 \text{ cm}^{-1}$ slice of the 2D anisotropy. These

results indicate that HB switching from a strained HB to a stable HB, on average, proceeds by an angular reorientation of $\geq 20^\circ$.

The frequency-dependent trends in our quadrant anisotropy results are consistent with the frequency-resolved narrow band pump-probe anisotropy trends that Bakker and co-workers observe, with red-to-red anisotropy being the highest and the blue-to-blue anisotropy being the lowest.¹⁹ However, our results do not display the timescales reported in their paper. Unlike the differences in picosecond timescales they report between the blue-to-blue and the red-to-red pump-probe anisotropies, we primarily see frequency dependence to anisotropy on much shorter inertial timescales. Our results are however consistent with broadband pump-probe anisotropy measurements by Moilenen et al.,¹⁸ where they also observe the largest frequency dependence in anisotropy to be during the < 100 fs inertial time period. The frequency dependent trends we see in our simulations and experiments on HOD/D₂O are in contrast with the narrow band pump-broadband probe experiments on HOD/H₂O by Bakker et al.,²⁰ where they report higher blue-to-blue anisotropy compared to blue-to-red anisotropy at a waiting time of 200 fs. Gaffney and co-workers have measured 2D difference spectra between parallel and perpendicular 2D IR spectra of aqueous ions in order to understand the kinetics of exchange via jump reorientation between ions and water molecules, and estimate these jump angles.^{11,12} They extract average jump angles of $\sim 50^\circ$ from their modeling of picosecond reorientation of water molecules switching to form HBs with ions. Since we adopt a different approach to extracting angles, and are primarily concerned with sub-picosecond inertial dynamics in water, we measure smaller cone angles for HB exchange in water.

IIIc. Comparison to MD Simulations

To better understand how the underlying hydrogen bond dynamics are reflected in the experiment, it is helpful to compare to the known dynamics of the SPC/E water model, which exhibits concerted hydrogen bond switching with jump reorientation.⁸ The mixed quantum-classical spectroscopic model used here has qualitatively reproduced many of the features of the OH vibrational spectroscopy,^{5,15,46,50} although the timescales for spectral relaxation are significantly shorter (600 fs¹⁵) than those observed in experiments.

Figure 2 (top right) shows simulated frequency-dependent pump-probe anisotropy calculated using methods described in section IIb. Simulated pump-probe anisotropy shows a <50 fs inertial component and a 2.3 ps long time relaxation, attributed to the collective reorientation of water molecules. Calculations of frequency-resolved P_2 and pump-probe anisotropy from MD simulations have been performed before using similar methodology.^{14,18,21,51} These calculations have revealed that the frequency dependence to orientational relaxation exists primarily during <50 fs inertial timescales, with negligible frequency dependence to the picosecond rotation dynamics, reflecting the fact that spectral diffusion timescales are faster than timescales of collective reorientation. Moreover, Lin et al. have pointed out that including the non-Condon effect and the 1-2 transition in a full response function calculation of pump-probe anisotropy diminishes the amplitude of the <50 fs inertial decay and consequently, raises the anisotropy values at longer waiting times.⁵¹ These calculations were shown to agree better with experimentally measured anisotropy compared to P_2 .

Similar to our analysis of experimental pump-probe anisotropy, we applied restricted rotation modeling to extract inertial angles from simulated pump-probe anisotropy. To be consistent with our analysis of the experimental data, we fit the simulated pump-probe anisotropy decay with a double exponential plus offset until a waiting time of 2.5 ps, with fixed timescales of 35 fs and 1.6 ps, varying only the amplitudes. Like in our experimental pump-probe anisotropy, the inertial decay amplitude increases with increasing detection frequency as displayed in the lower right panel of Figure 2. The bottom right panel of Figure 3 displays the calculated angles from simulated pump-probe anisotropy. The angles we extract from simulations vary in $\langle \theta \rangle$ from $\sim 3^\circ$ to $\sim 12^\circ$ and in $2\theta_H$ from $\sim 5^\circ$ to $\sim 20^\circ$, which are similar to the angles calculated from the experimental data. The resulting frequency dependence to the calculated inertial decay amplitudes shown in Figure 2 are also consistent with the trends calculated by Lin, et al. for the HOD/H₂O system. However, we see a steeper dependence of the inertial decay amplitude on detection frequency than reported in Ref 51. Laage and Hynes applied the hard cone model to <100 fs frequency dependent amplitudes from P_2 and calculated larger θ_0 ($2\theta_H$) – varying from 14° to 36° across the OH stretch band.²¹ The differences in the angles reported in these studies is likely due to the variations in the definitions used for the inertial reorientation amplitude.

Figures 6b and 7b show the 2D IR anisotropy of HOD/D₂O obtained from real and power spectra, respectively, calculated from MD simulations. The results in Figure 6b are consistent with previous calculations of anisotropy obtained from absorptive spectra.^{7,9} There are a number of qualitative similarities between the simulations and experiments, as well as some conspicuous quantitative differences. Both show that blue-

excitation followed by blue-detection leads to the lowest value anisotropies, while red-to-red anisotropies are highest. Similar to our experimental observations, the 2D anisotropy calculated from the power spectra are asymmetric about the diagonal, with slightly lower anisotropies observed in the blue-to-red quadrant compared to the red-to-blue quadrant. They share similar anisotropy contours, although the predicted values differ from experiment. The anisotropy values differ less from experiments at shorter waiting times than at longer waiting times. Also, for picosecond timescales, vertical contours are observed for blue-excitation, indicating that although some residual alignment still exists, memory of the initial frequency has vanished.

Figure 8 displays the experimental and simulated anisotropies from the four quadrants of the 2D anisotropy as a function of waiting time. Both experimental and simulated spectra tend toward the expected value of 0.4 at $\tau_2 = 0$, and show little indication of inertial response for time scales ≤ 100 fs. For both, the anisotropy decays observed for $\tau_2 < 400$ fs for red excitation is slower than for blue excitation, and relaxation for all quadrants occurs at the same rate by 1 ps. This confirms that the faster time scale of spectral diffusion acts to homogenize the observed relaxation considerably faster than orientational relaxation. It is also striking that the calculated 2D anisotropies show little <100 fs inertial response, when the calculated P_2 orientational correlation functions show a 25% decay within 100 fs,³⁶ with higher inertial contributions for blue excitation.^{14,21}

The differences between experimental and simulated spectra are most prominent at longer waiting times, where simulations underestimate the anisotropy amplitudes. The magnitude of orientational fluctuations at short times and the rate of orientational

relaxation as viewed through the 2D anisotropy are both higher in simulated spectra than in experiment. There are also different anisotropy contours observed in simulations for $\tau_2 < 200$ fs, where inertial reorientation dominates.

It is clear from these results that both experiments and simulation show 2D anisotropies with off-diagonal asymmetry, especially in those derived from power spectra. Within linear response and microscopic reversibility arguments, one expects red-to-blue and blue-to-red anisotropies to be equal. However it is difficult to discount the possibility that red-to-blue orientational relaxation has more HB fluctuations persisting about the stable linear configuration than the blue-to-red relaxation, leading to a smaller distribution of angles during the inertial period. This asymmetry could also be a result of blue excitation containing a significant fraction of bifurcated configurations, many of them switching, that undergoes large angle reorientation to return to a stable configuration.

In practice, quantitative analysis of polarization dependent nonlinear experiments is also complicated by interference effects between the $\nu = 0-1$ and $\nu = 1-2$ resonances. We used the simulations to better understand how the 2D spectral anisotropy can be distorted in different representations of the data. The 2D anisotropy from real and power spectra were also calculated for just the $\nu = 0-1$ transition (two-level system) using only the first term in eq. (1). Figure 10 compares the 2D anisotropy for the two-level and three-level systems calculated from real and power spectra. The 2D anisotropy derived from the real spectra using only the $\nu = 0-1$ transition is symmetric about the diagonal, as expected from the linear response approximation upon which these calculations are based. This is the most accurate representation of the orientational dynamics of the

model. However, for the same system, calculating the 2D anisotropy from power spectra breaks this symmetry as a result of the added contribution of the imaginary spectrum, which is not symmetric about the diagonal. This results in a higher red-to-blue anisotropy than what is measured in the blue-to-red quadrant. We also see that the anisotropy values along the diagonal are accurate, and the blue-to-red quadrant more faithfully reproduces the off-diagonal anisotropy from the real spectrum. The 2D anisotropy for the full three-level system from both real and power spectra are inherently asymmetric about the diagonal owing to the contribution from the anharmonically shifted $v=1-2$ transition. For the three-level system, the red-to-blue quadrant in the real spectra and the diagonal axis accurately reproduce the underlying dynamics seen in the two-level system. Since anisotropy calculated from power spectra for both the two- and three-level calculations are almost indistinguishable, the blue-to-red quadrant of the 2D anisotropy from power spectra most accurately reproduces the off-diagonal anisotropy in the two-level 2D anisotropy calculated from real spectra.

As another measure of how the experiment reflects the underlying angular changes, we applied the restricted orientation analysis to the 2D anisotropies calculated from simulations of the 2D IR real and power spectra at $\tau_2 = 96$ fs (Figure 9). Overall the average angular changes observed in experiments do not differ greatly from simulations. In both, average angular excursions for red and blue side excitation obtained from power spectra are roughly 6° and 12° , respectively. From the analysis of simulations, both real and power spectrum anisotropies predict similar inertial angular changes ($3-4^\circ$) across the OH lineshape. Like the experiments, the simulations predict an increase in average observed reorientation with detection frequency for red excitation in 2D experiments, and

in pump-probe anisotropies. However, the blue-to-red anisotropy remains fairly flat across ω_3 . These similarities seen in Figure 9 indicate that overall there is reasonable agreement between the inertial orientational dynamics in experiments and simulations.

This agreement between 2D anisotropy cone angles obtained from experiment and simulation is perhaps the best indication that the large angle reorientation during concerted HB switching seen in SPC/E water is consistent with the frequency dependent 2D anisotropies observed in simulations and experiments. The similarities in average angles plotted in Figure 9 show that, while these estimates seem to be small compared to the large angle reorientation predicted by earlier work on SPC/E water that reported switching angles of 50° or more,⁸ the values obtained from spectroscopic data are skewed by molecules that undergo translational or small-angle fluctuations. Unlike earlier simulation work that used geometric criteria to isolate switching events and extracted larger angles,⁸ our ability to window switching events is limited by the sensitivity of OH stretch frequencies to such events. Since the OH stretch frequency, especially on the blue-side of the lineshape, displays weaker correlation with HB angle and intermolecular separation distances,¹⁵ our analysis invariably includes fluctuations that do not involve successful switching of HB partners. We therefore find it useful to also look at two standard deviations in the harmonic cone model (Figure 9), which corresponds to 95% of the inertial angular excursions, since that better represents the larger rotations a water molecule initiating from a given configuration can undergo. The blue-to-red $2\theta_H$ half-angle of $\sim 15^\circ$ and a $3\theta_H$ half-angle of $\sim 23^\circ$ implies that $\sim 5\%$ of the molecules shifting from blue to red undergo full rotation of greater than 30° , with $\sim 0.3\%$ of excursions that we experimentally measure being larger than $\sim 46^\circ$.

Regardless of the agreement between the cone angles obtained from simulations and experiments in the present work, there are still several factors that are not accounted for in simulations, which must be kept in mind when comparing simulated and experimental spectra. One factor is that classical simulations do not treat librations quantum mechanically. Water's librational band in the infrared spans a range of frequencies ($\sim 300\text{-}1000\text{ cm}^{-1}$) that lie well above $k_B T$. Including quantum effects in describing librations have proven important for modeling infrared spectra and dielectric response.⁵⁵⁻⁵⁷ A recent study concluded that including nuclear quantum effects in simulation of water reorientation provided quantitatively accurate results for frequency and orientational correlations.^{53,54} A second factor to remember is that our simulations model the orientational relaxation of the OH bond vector of HOD/D₂O, while experiments track the rotation of the transition dipole moment of the HOD molecule. These are certainly not the same for the highly anharmonic OH stretch, and it has been seen that the angle between the transition dipole and the OH bond vector varies with the strength of the hydrogen bond.^{58,59} While the variation in this angle might be small across the OH stretch lineshape in the liquid phase, including this effect might lead to better agreement with experimental observations. Finally, these simulations were performed with the SPC/E rigid water model, which does not account for the bend-rotation coupling in the molecule and might predict large HB reorientation angles as a way of compensating for the model's inflexibility.

Two-dimensional anisotropy experiments provide a further criterion by which to judge the accuracy of hydrogen bond dynamics of water models. Most water models are not parameterized to account for dynamics, and show quantitative differences in spectral

diffusion and reorientation timescales.⁵⁰ A comparison of the model-dependent nature of calculated dynamical observables in a number of classical models have shown that the SPC/E model exhibits a better overall agreement with experiment at the qualitative level, but that polarizable models show closer agreement with experiment over timescales of structural relaxation.^{50,52} More recently, *ab initio* based water models propagated with centroid molecular dynamics showed better agreement with experimental reorientational and OH frequency correlation functions than classical MD simulations of rigid water models.^{53,54}

In making comparisons, it is important to note that even though the 2D anisotropy provides the most detailed constraints on switching dynamics, it is still a statistically averaged description of what may be a very heterogeneous process. Although one general mechanism for concerted switching has been characterized,⁸ other switching processes may be present to varying degrees. In fact, the analysis of the same SPC/E model using a different definition for a hydrogen bond, finds three distinct exchange processes of which 22% of switches do not follow the initially postulated jump reorientation.¹³ Experimental averaging over orientational motion along varying trajectories invariably complicates the microscopic interpretation of the pump-probe and 2D anisotropy measurements.

IV. CONCLUSIONS

We presented experimental and simulated 2D IR spectral anisotropy of the OH stretch of HOD/D₂O that directly reports on water reorientation during HB configurational changes. Experimental results show a frequency-dependent trend in anisotropy, whose behavior is consistent with the picture of large angle reorientation

during concerted hydrogen bond switching. We observe that strongly HB water molecules can be orientationally constrained for a few picoseconds, whereas molecules in broken or strained environments rapidly orientationally randomize. Given that 2D IR anisotropy can correlate HB configurational fluctuations with anisotropy, these experiments have allowed us to quantitatively approximate the angular rotation during hydrogen bond exchange, within the framework of restricted rotation models. From these calculations, we observe large angular deviations in the molecular dipole, as water molecules shift from a strained configuration to a stable configuration. This transition from a NHB to a HB configuration is characterized by a distribution of angles due to contributions from water molecules that undergo successful switches and those that do not. Average angles for water molecules relaxing from a NHB state to a stable HB state both from experiments and simulations were found to be 10° , leading to a full switching angle of at least 20° . Based on $3\theta_H$ values, we estimate the maximum angular deviations for a HB exchange event to be $\sim 46^\circ$. While these angles are smaller than the switching angles calculated from earlier simulation studies, our experiments are biased by the fraction of NHB molecules that do not successfully switch but undergo only translational and small-angle fluctuations to return to a HB state.

The increased orientational randomization of NHB molecules on inertial timescales as well as the rapid evolution of NHB molecules to a HB state observed in these experiments and simulations of the 2D anisotropy provide further confirmation that dangling hydrogen bonds do not persist in liquid water, that the HB structure remains largely tetrahedral on timescales of HB fluctuations, and that the concerted HB switching events involving multiple molecules proceed through a large change of HB angle.

Acknowledgements

This work was supported by the U.S Department of Energy (DE-FG02-99ER14988) and the ACS Petroleum Research Fund (46098-AC6). R.A.N. thanks the National Science Foundation for a Graduate Research Fellowship. K.R. thanks Carlos Baiz for a careful reading of the manuscript.

REFERENCES:

- 1 H. J. Bakker and J. L. Skinner, *Chem. Rev.* **110**, 1498-517 (2010).
- 2 I. Ohmine and H. Tanaka, *Chem. Rev.* **93**, 2545-2566 (1993).
- 3 F. H. Stillinger and T. A. Weber, *J. Phys. Chem.* **87**, 2833-2840 (1983).
- 4 F. H. Stillinger, *Science* **209**, 451-457 (1980).
- 5 J. D. Eaves, J. J. Loparo, C. J. Fecko, S. T. Roberts, A. Tokmakoff, and P. L. Geissler, *Proc. Natl. Acad. Sci. U.S.A.* **102**, 13019-22 (2005).
- 6 J. J. Loparo, S. T. Roberts, and A. Tokmakoff, *J. Chem. Phys.* **125**, 194522 (2006).
- 7 S. T. Roberts, K. Ramasesha, and A. Tokmakoff, *Acc. Chem. Res.* **42**, 1239-1249 (2009).
- 8 D. Laage and J. T. Hynes, *J. Phys. Chem. B* **112**, 14230-42 (2008).
- 9 G. Stirnemann and D. Laage, *J. Phys. Chem. Lett.* **1**, 1511-1516 (2010).
- 10 D. Laage and J. T. Hynes, *Science* **311**, 832-5 (2006).
- 11 M. Ji and K. J. Gaffney, *J. Chem. Phys.* **134**, 044516 (2011).
- 12 M. Ji, M. Odelius, and K. J. Gaffney, *Science* **328**, 1003-5 (2010).

- 13 R. H. Henchman and S. J. Irudayam, *J. Phys. Chem. B* **114**, 16792-810 (2010).
- 14 C. P. Lawrence and J. L. Skinner, *J. Chem. Phys.* **118**, 264 (2003).
- 15 J. D. Eaves, A. Tokmakoff, and P. L. Geissler, *J. Phys. Chem. A* **109**, 9424-36 (2005).
- 16 K. B. Møller, R. Rey, and J. T. Hynes, *J. Phys. Chem. A* **108**, 1275-1289 (2004).
- 17 K. Ramasesha, R. A. Nicodemus, S. T. Roberts, A. Mandal, and A. Tokmakoff, in *Ultrafast Phenomena XVII*, edited by M. Chergui, D. Jonas, E. Riedle, R. Schloenlein, and A. Taylor (Oxford University Press, 2010), pp. 454-456.
- 18 D. E. Moilanen, E. E. Fenn, Y.-S. Lin, J. L. Skinner, B. Bagchi, and M. D. Fayer, *Proc. Natl. Acad. Sci. U.S.A.* **105**, 5295-300 (2008).
- 19 H. J. Bakker, S. Woutersen, and H.-K. Neinhuys, *Chem. Phys.* **258**, 233-245 (2000).
- 20 H. J. Bakker, Y. L. A. Rezus, and R. L. A. Timmer, *J. Phys. Chem. A* **112**, 11523-34 (2008).
- 21 D. Laage and J. T. Hynes, *Chem. Phys. Lett.* **433**, 80-85 (2006).
- 22 C. J. Fecko, J. J. Loparo, and A. Tokmakoff, *Opt. Commun.* **241**, 521-528 (2004).
- 23 L. P. Deflores, R. A. Nicodemus, and A. Tokmakoff, *Opt. Lett.* **32**, 2966-8 (2007).
- 24 J. J. Loparo, S. T. Roberts, and A. Tokmakoff, *J. Chem. Phys.* **125**, 194521 (2006).
- 25 J. D. Hybl, A. Albrecht Ferro, and D. M. Jonas, *J. Chem. Phys.* **115**, 6606 (2001).
- 26 M. Khalil, N. Demirdöven, and A. Tokmakoff, *Phys. Rev. Lett.* **90**, 2-5 (2003).

- 27 J. A. Myers, K. L. M. Lewis, P. F. Tekavec, and J. P. Ogilvie, *Opt. Express* **16**, 17420-8 (2008).
- 28 R. A. Nicodemus, K. Ramasesha, S. T. Roberts, and A. Tokmakoff, *J. Phys. Chem. Lett.* **1**, 1068-1072 (2010).
- 29 Y. L. A. Rezus and H. J. Bakker, *J. Chem. Phys.* **125**, 144512 (2006).
- 30 C. J. Fecko, J. J. Loparo, S. T. Roberts, and A. Tokmakoff, *J. Chem. Phys.* **122**, 54506 (2005).
- 31 S. Yeremenko, M. Pshenichnikov, and D. Wiersma, *Phys. Rev. A* **73**, 2-5 (2006).
- 32 C. J. Fecko, J. D. Eaves, J. J. Loparo, A. Tokmakoff, and P. L. Geissler, *Science* **301**, 1698-1702 (2003).
- 33 J. J. Loparo, S. T. Roberts, R. A. Nicodemus, and A. Tokmakoff, *Chem. Phys.* **341**, 218-229 (2007).
- 34 A. Piryatinski and J. L. Skinner, *J. Phys. Chem. B* **106**, 8055-8063 (2002).
- 35 J. R. Schmidt, S. A. Corcelli, and J. L. Skinner, *J. Chem. Phys.* **123**, 044513 (2005).
- 36 J. J. Loparo, C. J. Fecko, J. D. Eaves, S. T. Roberts, and A. Tokmakoff, *Phys. Rev. B* **70**, 1-4 (2004).
- 37 C. C. Wang and R. Pecora, *J. Chem. Phys.* **72**, 5333-5340 (1980).
- 38 G. Lipari and A. Szabo, *J. Am. Chem. Soc.* **104**, 4546-4559 (1982).
- 39 G. Lipari and A. Szabo, *Biophys. J.* **30**, 489-506 (1980).
- 40 H. Tanaka and I. Ohmine, *J. Chem. Phys.* **87**, 6128 (1987).
- 41 I. Ohmine and S. Saito, *Acc. Chem. Res.* **32**, 825-825 (1999).

- 42 G. E. Walrafen, Y. C. Chu, and G. J. Piermarini, *J. Phys. Chem.* **100**, 10363-10372 (1996).
- 43 G. E. Walrafen, *J. Chem. Phys.* **121**, 2729-36 (2004).
- 44 C. J. Fecko, J. D. Eaves, and A. Tokmakoff, *J. Chem. Phys.* **117**, 1139 (2002).
- 45 S. T. Roberts, J. J. Loparo, and A. Tokmakoff, *J. Chem. Phys.* **125**, 084502 (2006).
- 46 J. B. Asbury, T. Steinel, C. Stromberg, S. A. Corcelli, C. P. Lawrence, J. L. Skinner, and M. D. Fayer, *J. Phys. Chem. A* **108**, 1107-1119 (2004).
- 47 P. Hamm, *J. Chem. Phys.* **124**, 124506 (2006).
- 48 A. Tokmakoff, *J. Chem. Phys.* **105**, 1 (1996).
- 49 A. Tokmakoff and M. D. Fayer, *J. Chem. Phys.* **103**, 2810 (1995).
- 50 J. R. Schmidt, S. T. Roberts, J. J. Loparo, A. Tokmakoff, M. D. Fayer, and J. L. Skinner, *Chem. Phys.* **341**, 143-157 (2007).
- 51 Y.-S. Lin, P. A. Pieniazek, M. Yang, and J. L. Skinner, *J. Chem. Phys.* **132**, 174505 (2010).
- 52 E. Harder, J. D. Eaves, A. Tokmakoff, and B J Berne, *Proc. Natl. Acad. Sci. U.S.A.* **102**, 11611-11616 (2005).
- 53 F. Paesani, *J. Phys. Chem. A* **115**, 6861-6871 (2011).
- 54 F. Paesani, S. Yoo, H. J. Bakker, and S. S. Xantheas, *J. Phys. Chem. Lett.* **1**, 2316-2321 (2010).
- 55 P. A. Bopp, A. A. Kornyshev, and G. Sutmann, *Chem. Phys.* **109**, 1939-1958 (1998).
- 56 P. Luigi, M. Bernasconi, and M. Parrinello, *Chem. Phys. Lett.* **2614**, (1997).

- 57 B. Guillot, J. Chem. Phys. **95**, 1543 (1991).
- 58 E. Whalley and D. D. Klug, J. Chem. Phys. **84**, 78-80 (1985).
- 59 J. R. Fair, O. Votava, and D. J. Nesbitt, J. Chem. Phys. **108**, 72 (1998).

Figures:

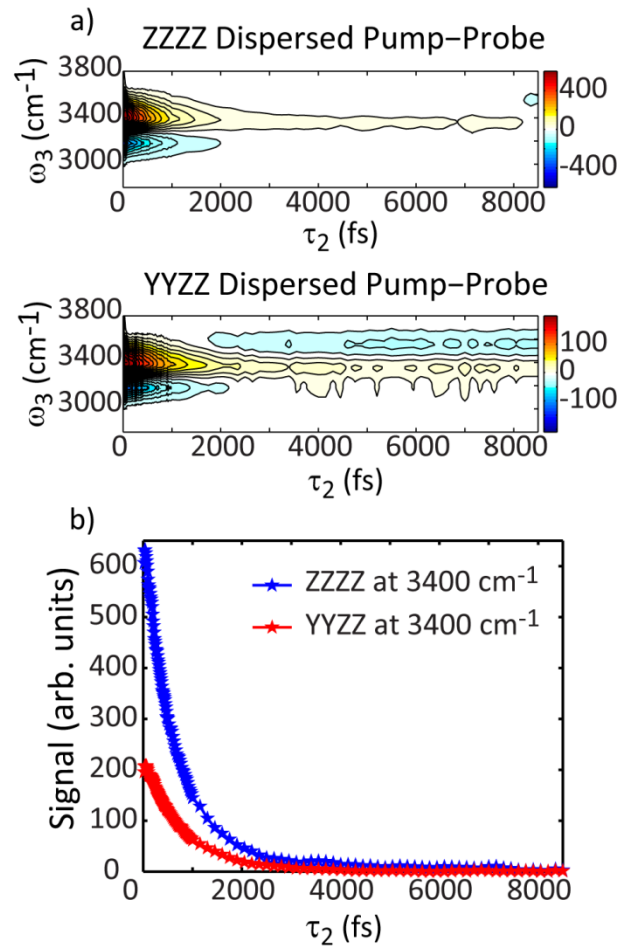


Figure 1: (a) Raw ZZZZ and YZZZ dispersed pump-probe of HOD/D₂O plotted against waiting time (τ_2), before TSGS correction; (b) 3400 cm⁻¹ slice of the ZZZZ and YZZZ dispersed pump-probe, after correcting for TSGS. A three-point rolling average was performed for waiting times of <400 fs.

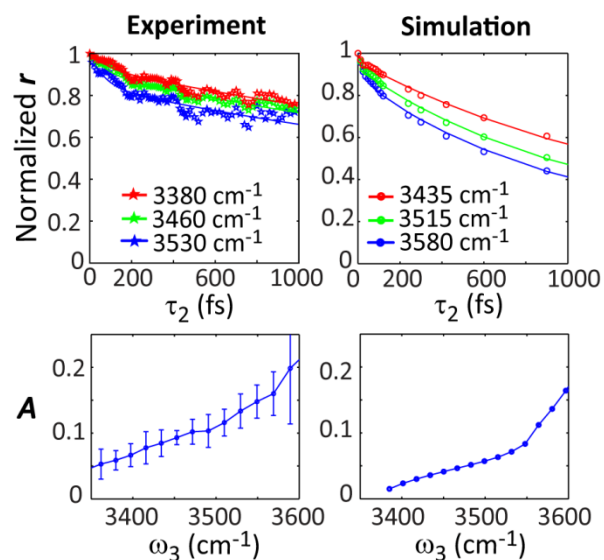


Figure 2: Experimental (left) and simulated (right) normalized pump-probe anisotropy of HOD/D₂O and the specified probe frequencies. The experimental traces were fit to a double exponential plus offset, with timescales of 70 fs and 2.7 ps, and pump-probe anisotropy from simulations were fit to the same function with timescales of 35 fs and 1.5 ps . For the experimental data, a rolling average was performed for short time delays, upon subtracting the hot ground state contribution from ZZZZ and YYZZ spectra; Lower panel shows the amplitude of the inertial decay as a function of probe frequency. Error bars in the experimental plot indicate the standard deviation across four independent measurements

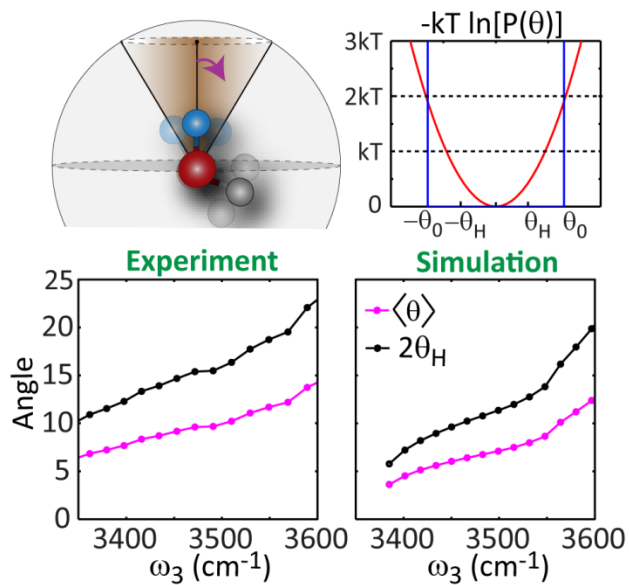


Figure 3: Cartoon of restricted rotation model (top left). Potential of mean force for the hard cone (blue) and the harmonic cone (red) models (top right). Average angles and two standard deviations of the half-cone angle calculated from the inertial decay of measured and simulated pump-probe anisotropy (bottom), based on harmonic cone analysis.

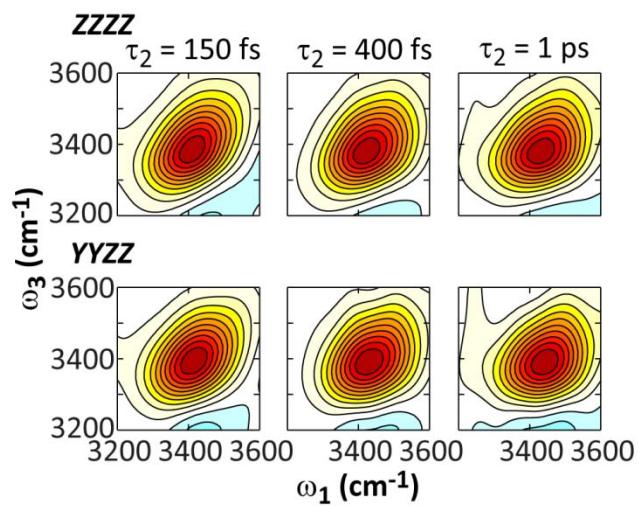


Figure 4: 2D IR surfaces of HOD in D₂O in the ZZZZ and YYZZ polarization geometries, normalized to their maximum amplitudes, with linearly spaced contours. The ratio of the maximum amplitude of ZZZZ to ZZYY at 150 fs was 2.94.

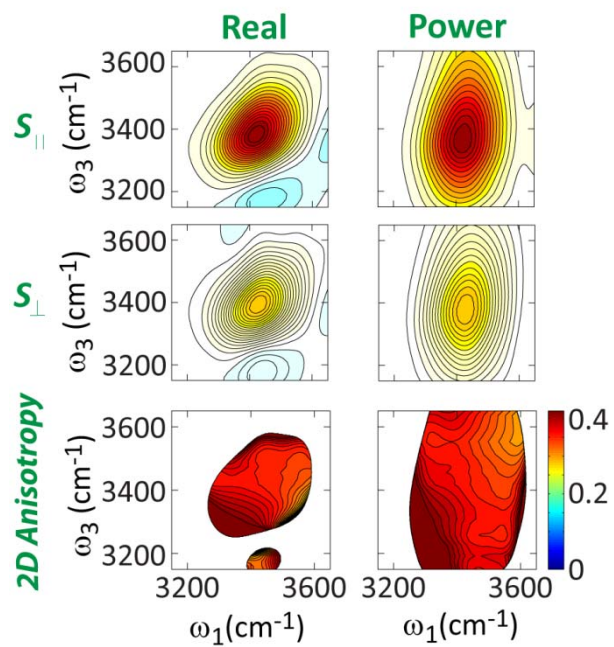


Figure 5: Absorptive (left) and power (right) 2D IR spectra of HOD in D₂O at $\tau_2 = 250$ fs, for ZZZZ (top row) and YZZZ (second row) polarizations. Corresponding 2D IR anisotropy calculated from real absorptive (bottom left) and power (bottom right) spectra. Contours represent a change in anisotropy of 0.01.

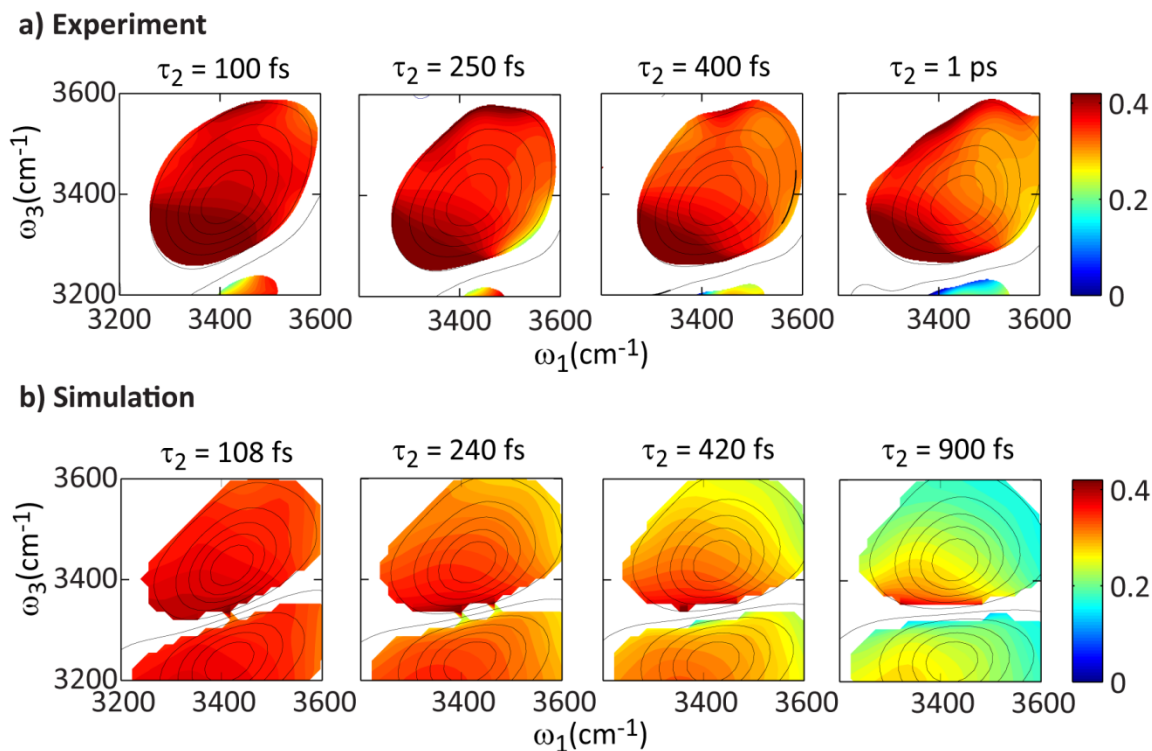
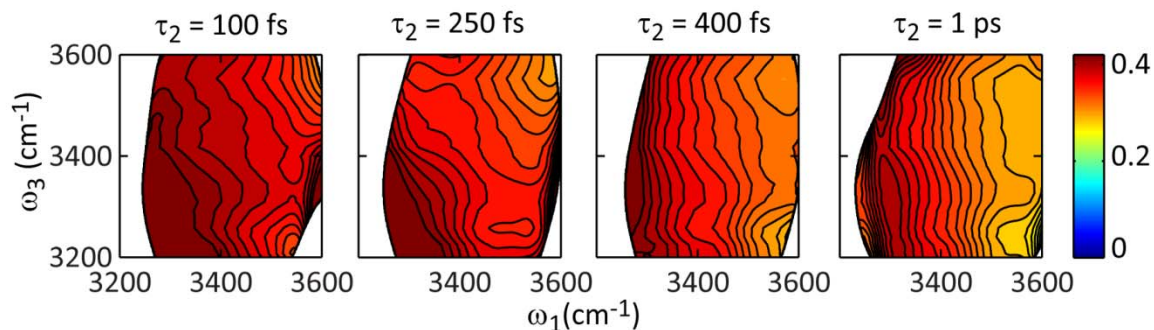


Figure 6: 2D IR anisotropy spectra of HOD/D₂O calculated from absorptive ZZZZ and YYZZ 2D IR spectra from (a) experiment and (b) simulations, at four different waiting times. Anisotropy is color-coded to represent a change of 0.01, and contour lines show the shape of the underlying isotropic spectra. These spectra have been truncated to eliminate (ω_1, ω_3) data points where the magnitude of the isotropic response is less than 8% of its maximum value.

a) Experiment



b) Simulation

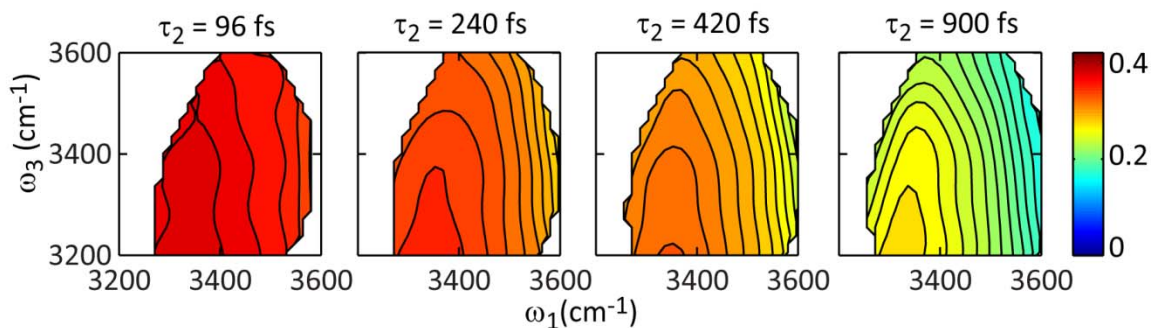


Figure 7: 2D IR anisotropy spectra for HOD in D₂O from (a) experiment and (b) simulation, at various waiting times. Each contour represents a change in anisotropy of 0.01. These spectra have been truncated to eliminate (ω_1 , ω_3) data points where the magnitude of the isotropic response is less than 10% of its maximum value.

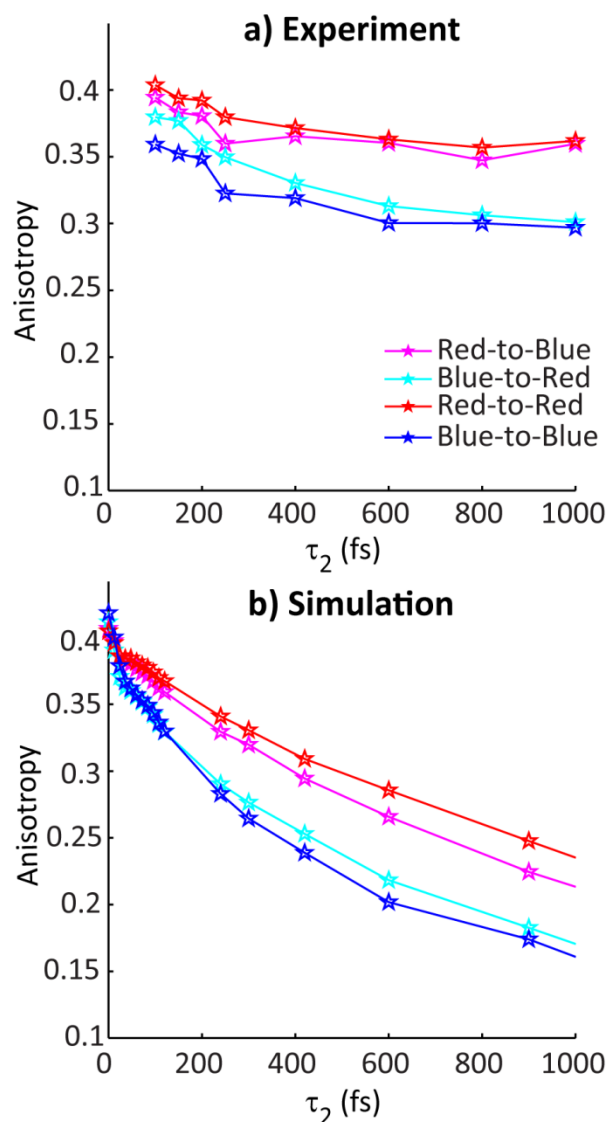


Figure 8: (a) Experimental and (b) simulated waiting time behavior of the four quadrants of the 2D IR anisotropy calculated from 2D IR power spectra. These quadrant anisotropies were calculated by integrating a 50 cm^{-1} -by- 50 cm^{-1} box in corresponding quadrants of the 2D anisotropy surface, and normalizing to the number of data points in the respective box. “Red” refers to $3350\text{-}3400 \text{ cm}^{-1}$ for experimental anisotropies and $3400\text{-}3450 \text{ cm}^{-1}$ for the simulated anisotropies (to account for the shifted OH stretch absorption in simulations). “Blue” refers to $3500\text{-}3550 \text{ cm}^{-1}$ for experiments and $3550\text{-}3600 \text{ cm}^{-1}$ for simulated anisotropies.

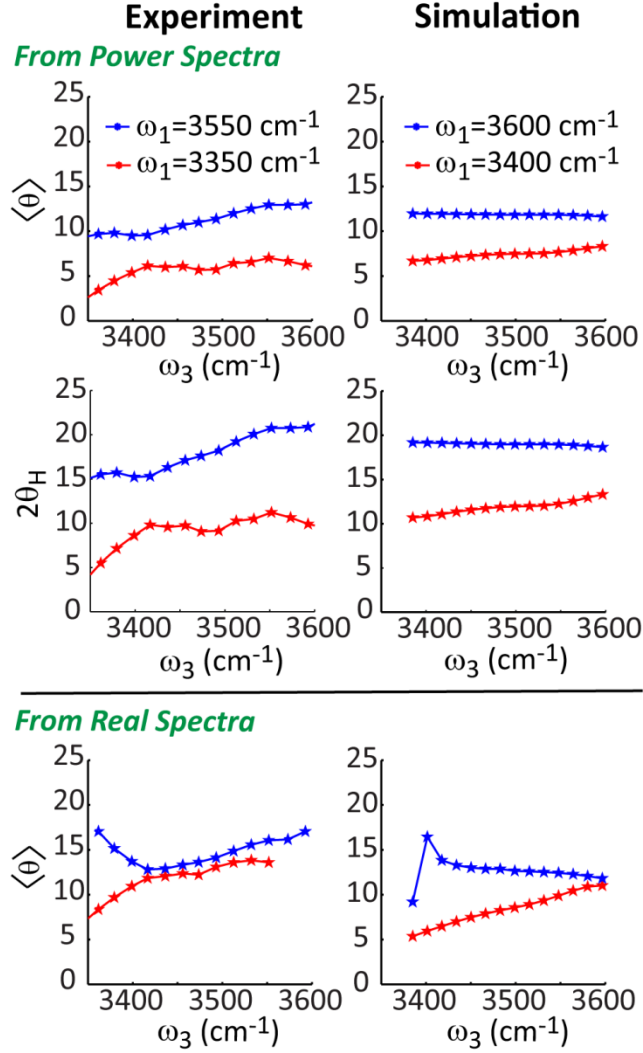


Figure 9: Average angular deviations extracted from ω_1 = “red” and ω_1 = “blue” slices of 2D IR anisotropy from experiment (left) and simulation (right), at $\tau_2=100$ fs using the harmonic cone model. Average angles (top row) and two standard deviations (middle row) were calculated based on 2D IR anisotropy from power spectra. Average angles from 2D IR absorptive spectra are also shown (bottom row). Average angles calculated from the hard cone model (not shown) are close-to identical to those calculated from the harmonic cone model. Also, we found that the hard cone angle $\theta_0 \approx 2\theta_H$.

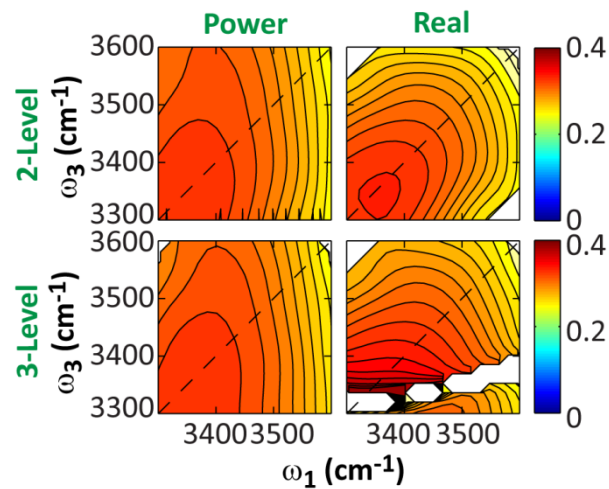
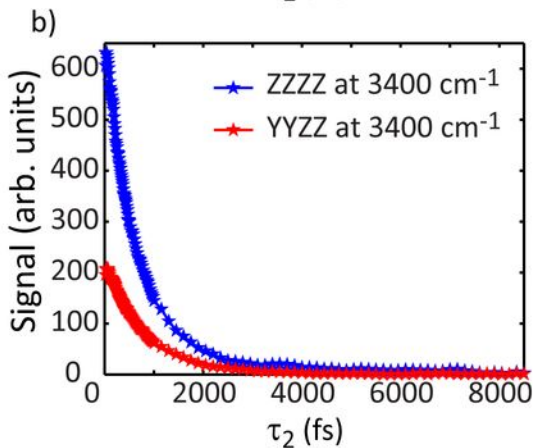
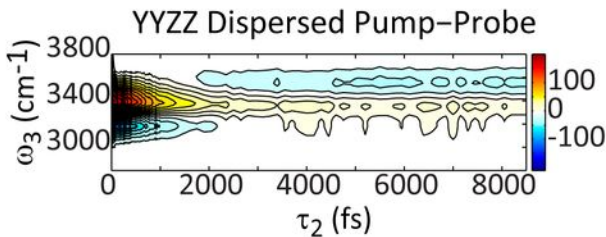
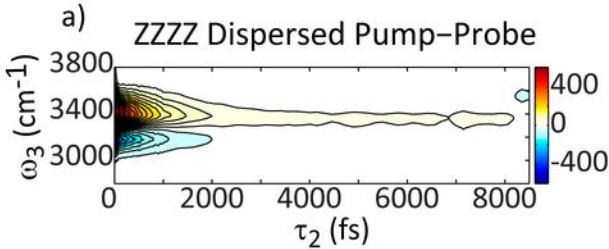
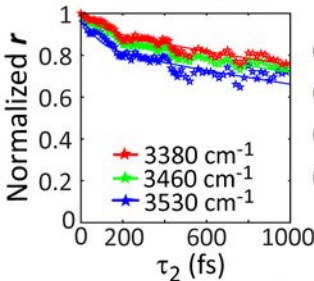
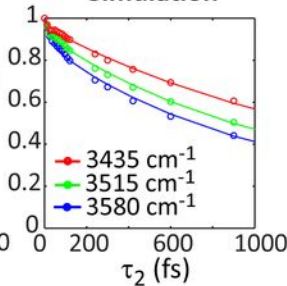
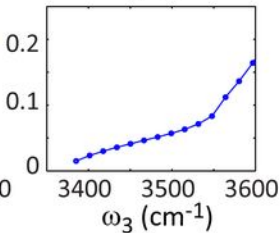
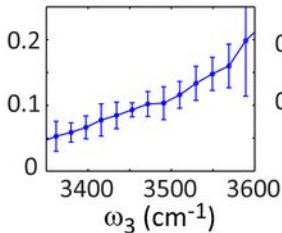
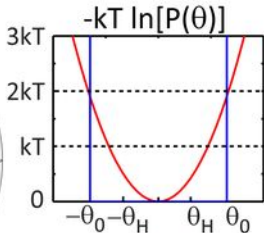
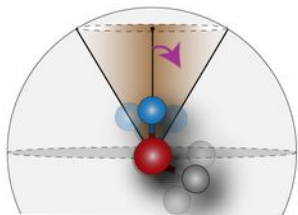


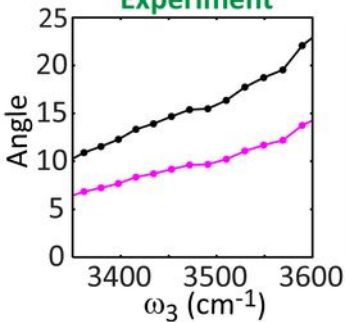
Figure 10: Comparison of different representations of 2D IR anisotropy from simulations at $\tau_2 = 300$ fs. 2D anisotropy for the two-level system (not including the $v = 1-2$ transition) are shown in the upper row, and 2D anisotropy for the three-level system are shown in the bottom row. 2D anisotropy for each system was calculated both from the absorptive (left) and power (right) 2D IR spectra. Each contour represents a change in anisotropy of 0.01.



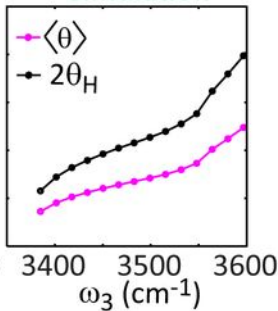
Experiment**Simulation****A**

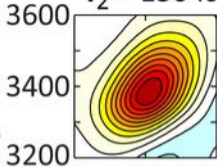
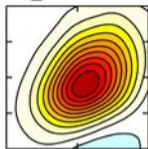
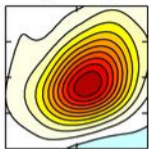
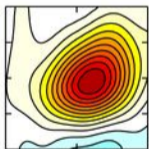
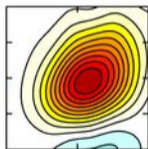
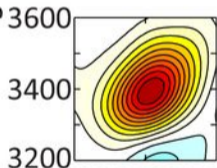


Experiment



Simulation



ZZZZ $\tau_2 = 150$ fs $\tau_2 = 400$ fs $\tau_2 = 1$ ps**YYZZ** ω_3 (cm⁻¹)

3200 3400 3600

3400 3600

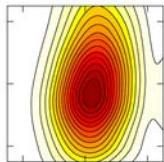
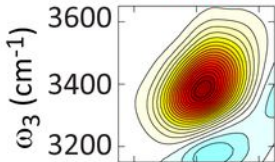
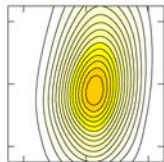
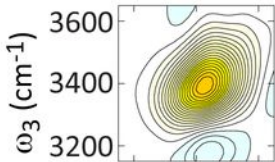
3400 3600

 ω_1 (cm⁻¹)

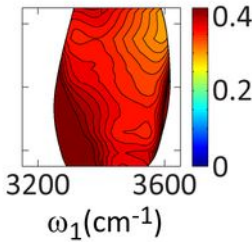
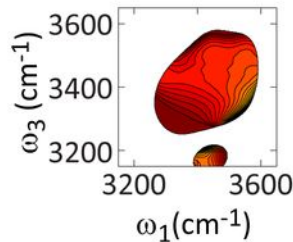
$S_{||}$

Real

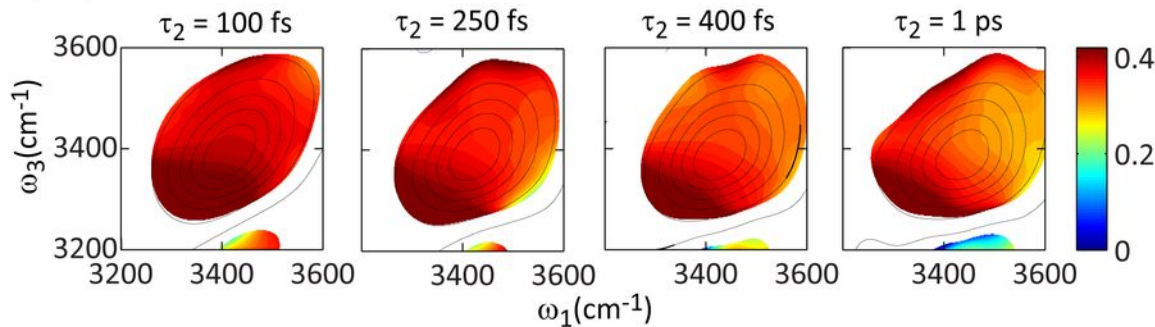
Power

 S_{\perp} 

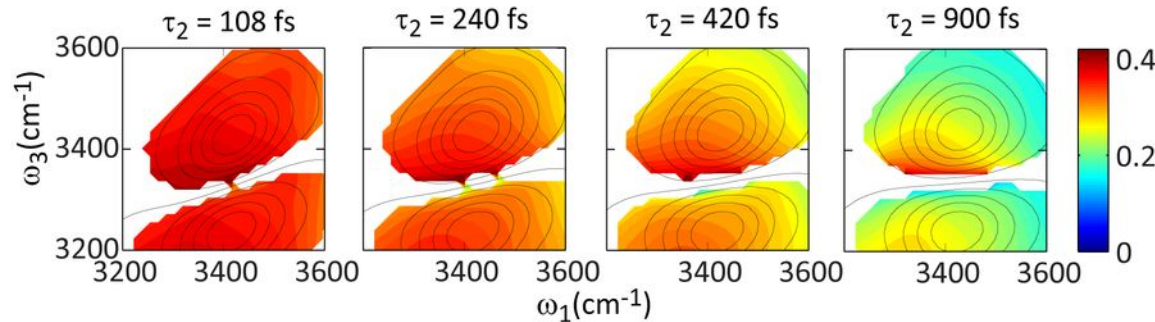
2D Anisotropy



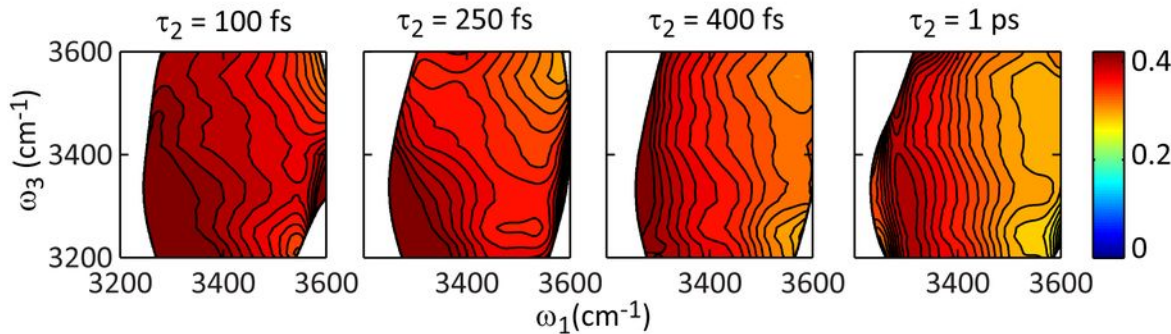
a) Experiment



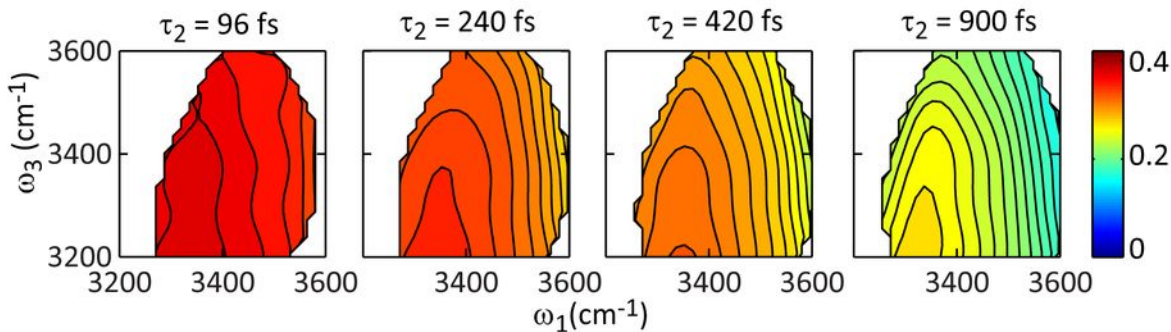
b) Simulation



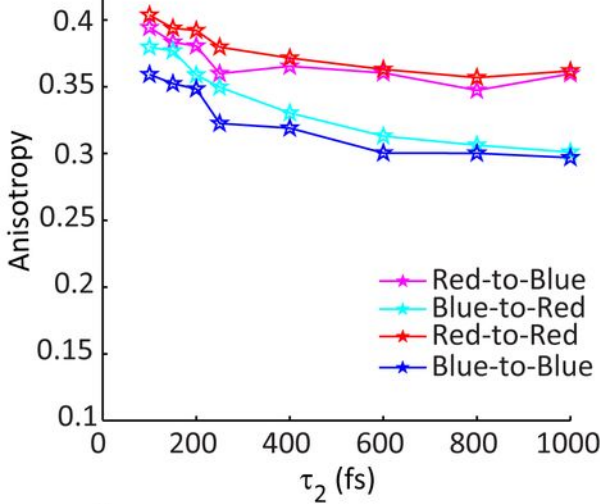
a) Experiment



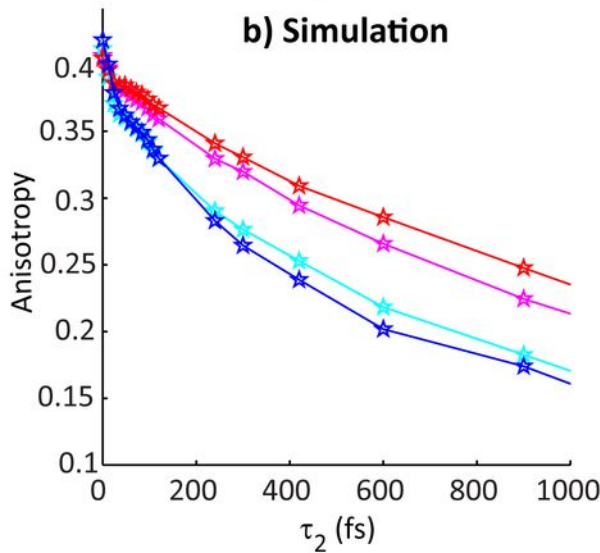
b) Simulation



a) Experiment



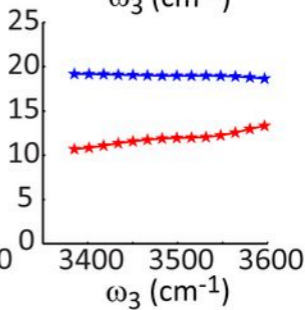
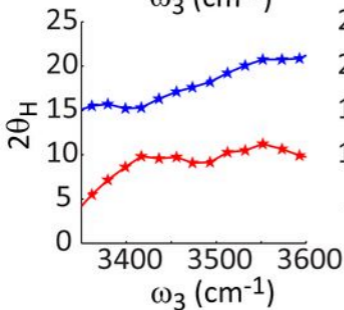
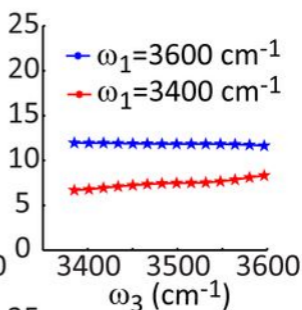
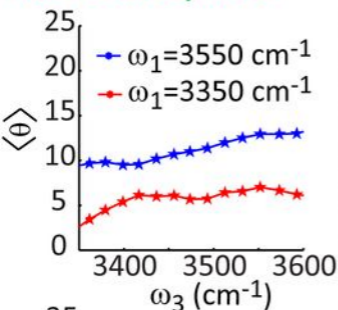
b) Simulation



Experiment

Simulation

From Power Spectra



From Real Spectra

